weak inertial oscillations (the local inertial period is 14.8 hours), but otherwise $R_{u'u'}$ and $R_{v'v'}$ fall off more or less exponentially with time, with an *e*-folding time of 15 hours. The lagged cross-correlation between u' and v' shows the weak clockwise-rotating inertial oscillations and an indication of more counterclockwise than clockwise energy at lower frequencies.

The autocorrelations lead to a particularly simple statistical scheme for operational trajectory prediction (*10*) and also imply a horizontal diffusivity (*11*) of 1100 m^2/sec on this part of the Labrador Shelf. This estimate is slightly in error because the influence of the wind prevents the icebergs from following the current perfectly. Using length scales determined from an Eulerian analysis (see below), we estimate that this has reduced the Lagrangian autocorrelation time by about 1 hour, so that the eddy diffusivity should be about 1200 m^2/sec.

We have more than 6000 values of the residual velocity (u', x, t) at GUDRID. We first referred these to a frame of reference moving with the mean flow and then evaluated the correlation functions $f\star(r,\tau)$, $g\star(r,\tau)$ of longitudinal and transverse velocity components, respectively (*12*), for spatial separation r and time lag τ. In doing this we multiplied together all velocity pairs for different icebergs and accumulated them in bins of size 2 hours (as for the autocorrelation) by 3.7 km. We also evaluated the lagged cross-correlation between longitudinal and transverse velocity components; this shows the effects of inertial motion, but is relatively small and is not discussed further here.

We found that $f\star$ and $g\star$ are reasonably separable into

$$f\star(r,\tau) = f(r)F(\tau)$$

$$g\star(r,\tau) = g(r)G(\tau)$$

These functions are shown in Figs. 4 and 5.

Nondivergent two-dimensional turbulence would have $g = d(rf)/dr$ (*13*), and the data are not inconsistent with this. The length scale of the eddies, from the value of r for which $g(r) = 0$, is 31 km, comparable with the length scale of shelf-edge eddies observed in satellite imagery (*14*).

The integral time scale (from an average of $F(\tau)$ and $G(\tau)$ in Fig. 5) is about 40 hours, considerably longer than the corrected Lagrangian time scale of 16 hours, as predicted theoretically (*15*).

The functions $f\star(r,\tau)$ and $g\star(r,\tau)$, with or without the assumption of separability, can be Fourier-transformed into the wavenumber-frequency energy spectrum of the eddy field (*16*). We emphasize that, as elsewhere (*13*), drifter data can provide information that is not readily obtainable from moored current meters.

CHRISTOPHER GARRETT
JOHN MIDDLETON
MARK HAZEN
FOUAD MAJAESS

Department of Oceanography, Dalhousie University, Halifax, Novia Scotia, Canada B3H 4J1

References and Notes

1. For a general review of the operational problems, see J. D. Miller and M. J. Dillon [*J. Can. Pet. Technol.* **23**, 45 (1984)].
2. Data for 1974 to 1979 were compiled by the Atmospheric Environment Service and were provided to us by S. D. Smith of Bedford Institute. J. R. Buckley of PetroCanada provided the data for 1980 and 1981.
3. Correction for nodal factors and conversion to Greenwich phase lag follow the procedure described in the tidal manual of the Canadian Hydrographic Service.
4. D. B. Fissel and D. D. Lemon, "Analysis of physical oceanographic data from the Labrador shelf, summer 1980" (report published by Arctic Sciences Ltd., Sidney, British Columbia, 1982), vols. 1 and 2.
5. J. R. Buckley, personal communication.
6. Draft estimates were made for about 25 percent of the icebergs tracked, giving a mean draft of 75 m; this is probably an overestimate (J. D. Miller, personal communication).
7. V. R. Swail and A. Saulesleja, "Geostrophic wind climatology of the Northwest Atlantic Ocean" (Canadian Climate Centre Report 81/6, 1981). A data tape was provided to us by B. D. Petrie of Bedford Institute.
8. K. R. Thompson, R. F. Marsden, D. G. Wright, *J. Phys. Oceanogr.* **13**, 1003 (1983).
9. S. D. Smith and E. G. Banke, *Cold Regions Sci. Technol.* **6**, 241 (1983).
10. C. J. R. Garrett, *Iceberg Res.* **7**, 3 (1984).
11. G. I. Taylor, *Proc. London Math. Soc. Ser. A*, **20**, 196 (1921).
12. G. K. Batchelor, *The Theory of Homogeneous Turbulence* (Cambridge Univ. Press, Cambridge, 1960).
13. H. J. Freeland, P. B. Rhines, T. Rossby, *J. Mar. Res.* **33**, 383 (1975).
14. P. H. LeBlond, *Atmos.-Ocean* **20**, 129 (1982).
15. J. F. Middleton, *J. Mar. Res.* in press.
16. ______ and C. J. R. Garrett, in preparation.

17. We thank numerous anonymous ice observers who collected the original data provided to us by S. D. Smith and J. R. Buckley. We thank S. D. Smith, J. R. Buckley, J. D. Miller, and B. D. Petrie for discussions. Supported by a contract from the Department of Supply and Services and by the Natural Sciences and Engineering Research Council.

25 July 1984; accepted 22 October 1984

Rheology of Glacier Ice

Abstract. *A new method for calculating the stress field in bounded ice shelves is used to compare strain rate and deviatoric stress on the Ross Ice Shelf, Antarctica. The analysis shows that strain rate (per second) increases as the third power of deviatoric stress (in newtons per square meter), with a constant of proportionality equal to 2.3 × 10^{-25}.*

Glaciers flow under gravitationally induced stresses. The weight of the ice causes the glacier to spread and thin in a manner dictated by surface conditions, basal conditions, and the ice constitutive relation between strain rate and applied stress. Because of the complex interaction of these three elements within the glacier and because of the difficulty of simulating intraglacial conditions in the laboratory, the constitutive relation is still an issue in glaciology.

Laboratory investigations (*1, 2*) have yielded a power-law relation between the steady-state effective strain-rate ($\dot{\epsilon}$) and the effective deviatoric stress (τ), such that

$$\dot{\epsilon} = A\tau^n \quad (1)$$

where $\dot{\epsilon}$ and τ are defined so as to be invariant under coordinate system rotation (*3*). The ice-flow law constant A is affected by ice fabric and impurity content and exhibits an Arrhenius-type temperature dependence. The value of n is approximately 3, but laboratory experiments are inconclusive for $\tau < 1$ bar and at temperatures less than -10°C—the typical stress and temperature regime of polar glaciers—because strain rates are very small and it is difficult to distinguish steady-state creep from transient creep. Consequently, information on the low-stress rheology of ice is best obtained from observations of glacier behavior. These observations are needed also to detect whether the fabric of glacier ice (grain size, crystal orientation, and so on) significantly affects ice rheology.

Studies of the closure of boreholes and tunnels in glacer ice (*3*) and of ice-rise morphology (*4*) have yielded in situ estimates of A and n. Results are ambiguous, however, due mainly to uncertainties in associated estimates of basal temperatures and of stresses within the ice. Less ambiguous results have been obtained from ice shelves—floating platforms of thick ice that are extensions of the inland ice sheet over the ocean. There is no friction at the base of an ice shelf. Thus, strain rates measured at the surface are characteristic of the entire thickness, and the spreading stress (T) in a freely floating ice shelf can be expressed simply (*5*) in terms of ice thickness (H), the acceleration due to gravity (g) and the densities of seawater (ρ_w) and ice (ρ_i)

$$T = \frac{1}{2}\frac{\rho_i}{\rho_w}(\rho_w - \rho_i)gH \quad (2)$$

Moreover, the basal temperature is constrained to be the freezing point of seawater.

Analysis of strain rate and ice-thickness measurements from several ice shelves has yielded estimates of n and A for the stress range 0.1 through 1 bar (6), but the analysis was restricted to regions where creep appeared to be unaffected by drag between the floating ice shelf and either its grounded margins or localized grounded areas (ice rises). These grounded areas exert a back stress (σ_b) on the ice shelf, reducing creep rates. Ice rises are of particular interest because it is believed that they regulate not only the flow of ice shelves but also the flow of many Antarctic glaciers that drain into ice shelves (7). We present a method of estimating the flow properties of ice shelves affected by such grounded areas.

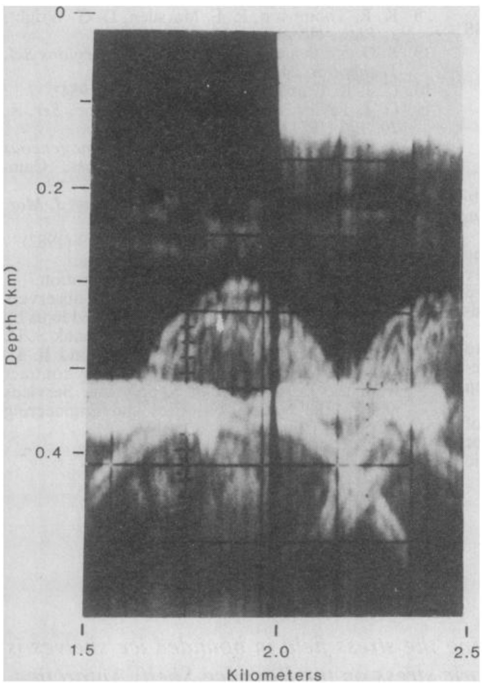

Fig. 1. Radar echogram collected at a station in the central region of the Ross Ice Shelf (7.5° grid south and 1.5° grid west) (Fig. 2). The ice thickness is about 420 m and the ice-seawater interface appears as the strong, nearly horizontal reflector at that depth. Bottom crevasses appear as large diffraction hyperbolas. The height of the apex of the hyperbola gives the height of the crevasse. In this case the height is about 120 m.

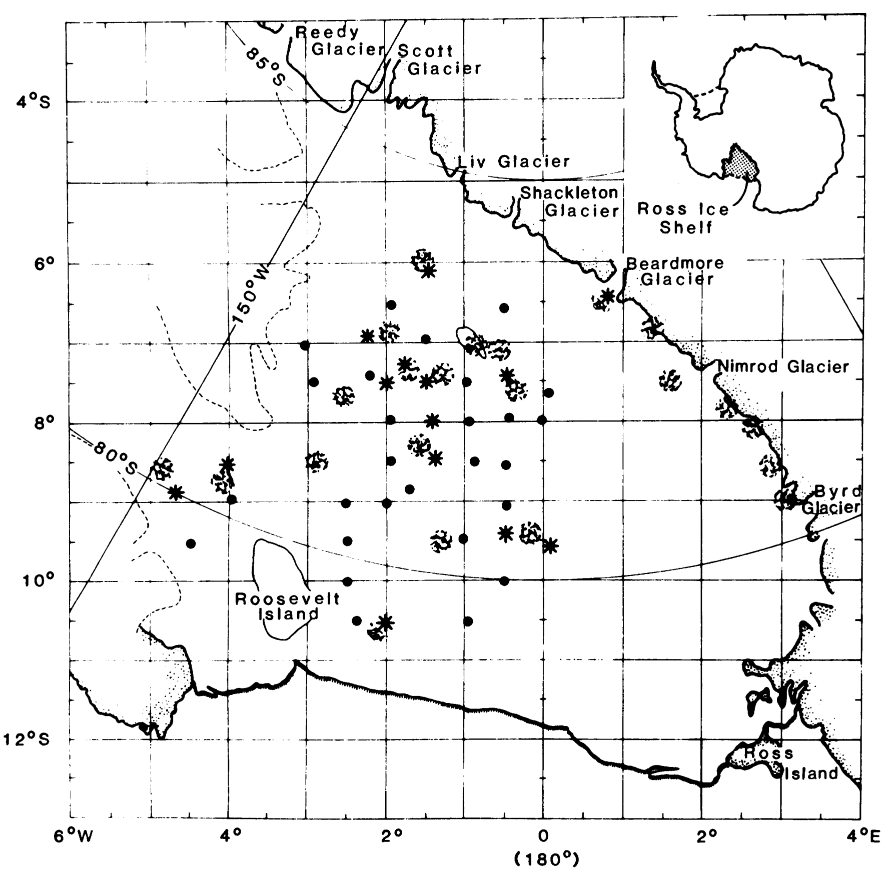

Fig. 2. Map of the Ross Ice Shelf showing the locations of the centers of bottom crevasse fields (mottled patches) and of surface strain-rate measurements (stars and circles). The stars correspond to locations where we have our best estimates of back stress. The insert map shows Antarctica and the Ross Ice Shelf.

For an ice shelf where creep is restricted by drag at the margins or at ice rises, τ in Eq. 1 is given by

$$\tau = \frac{(1 + \alpha + \alpha^2 + \beta^2)^{1/2}}{2 + \alpha} (T + \sigma_b) \tag{3}$$

where α and β are ratios between horizontal components of the strain-rate tensor with $\alpha = \dot{\epsilon}_{yy}/\dot{\epsilon}_{xx}$ and $\beta = \dot{\epsilon}_{xy}/\dot{\epsilon}_{xx}$; σ_b is a negative, compressive stress and serves to reduce the spreading stress T; and the expression applies regardless of the choice of x-axis. Equations 1 and 3 have been used to estimate σ_b on the Ross Ice Shelf from measurement of strain rate, ice thickness, and surface temperature (8). Values of A and n were selected on the basis of other measurements. More recently, Jezek (9) has shown that σ_b can be deduced from measurement of the height of bottom crevasses, which are fractures that extend upward into ice shelves. They form when seawater penetrates into the base of the ice shelf and ruptures the ice up to the level at which englacial stresses equal the stress exerted by seawater. The crevasses are clearly visible on radar reflection records and penetration height can be estimated from these records (Fig. 1).

Jezek's analysis is based on an earlier theory by Weertman (10) for calculating the height of an isolated crevasse. By assuming that the crevasses open along a principal stress axis (hence β in Eq. 3 is 0, and the derived σ_b acts perpendicular to the crevasse), Jezek showed that

$$\sigma_b = \frac{2\,(\rho_w - \rho_i)}{\pi} gL - T \tag{4}$$

where L is the height of the bottom crevasse. Substituting Eq. 4 into Eq. 3 gives

$$\tau = \frac{(1 + \alpha + \alpha^2)^{1/2}}{2 + \alpha} \left[\frac{2\,(\rho_w - \rho_i)}{\pi} \right] gL \tag{5}$$

This equation relates the height of bottom crevasses to the effective stress in a bounded ice shelf. It does not imply that the effective stress is 0 in regions of an ice shelf where there are no crevasses, because crevasses form only when a preexisting crack of a critical length is already present. Such planes of weakness may be initiated as ice flows over and around grounded zones; basal crevasses often form downstream from such areas (*11*).

Equations 1, 3 and 4 allow us to calculate the constants n and A from measured strain rates and values of σ_b deduced from measured crevasse heights on the Ross Ice Shelf (Fig. 2). Our analysis is limited to regions where bottom crevasses form, typically downstream of pinning points.

In general, measurements of strain rates were not made close to bottom crevasses. Consequently, we interpolated values of the back stress (σ_b) from contoured estimates of σ_b derived from measurements of bottom crevasse heights (*9*). Interpolations were not accepted from areas where contours were uncertain because of sparse measurements of complex flow, nor from areas where the contours were closely spaced. In the remaining areas, we interpolated σ_b to the sites of strain-rate measurements, calculated τ from Eq. 3, and calculated $\dot{\epsilon}$ from the measured surface strain-rate data. Figure 3 shows the results with log $\dot{\epsilon}$ plotted as a function of log τ and estimated error bars on the "best" data. These were selected by assessing regional consistency of σ_b values and proximity of basal crevasses to sites where strain rates were measured. Errors include uncertainties of ± 0.02 MN m^{-2} in σ_b and $\pm 1.5 \times 10^{-12}$ per second in measured strain rates (*12*).

The least-squares regression line fitted to the best data has a slope of $n = 3.3$, with limits of 2.8 and 4.1 for 1 standard deviation of the sample. In order to compare values of the constant A from these results with those from other studies, we follow previous investigators (*1*, *6*) in setting $n = 3$. Solution of Eq. 1 for the starred data points in Fig. 3 then gives $\bar{A} = (2.3 \pm 1) \times 10^{-25}$ sec^{-1} (N m^{-2})$^{-3}$, where $\bar{A}$ is the mean value of depth-averaged values of A at the Ross Ice Shelf stations (Fig. 2).

The temperature dependence of A can be represented as $A = A_o \exp(-Q/RT)$, where A_o is constant, Q is the activation energy for creep, R is the gas constant, and T is temperature in degrees Kelvin. Thomas and MacAyeal (*8*) modelled temperatures within the ice shelf and used these to calculate values of A at Ross Ice Shelf stations where strain rates were measured. They assumed $n = 3$ and adopted values of Q and A_o consistent with laboratory experiments and other measurements of ice-shelf creep. Within the region covered by our study, they obtained values of $\bar{A}$ in the range (1.5 to 3.0) $\times 10^{-25}$ sec^{-1} (N m^{-2})$^{-3}$. This is in excellent agreement with our result and indicates that the scatter in our data may be partly due to temperature variation across the ice shelf.

Our data also serve to highlight the influence of σ_b on the creep behavior of the Ross Ice Shelf. If σ_b is assumed to be identically 0 everywhere, then the calculated values of log τ (Fig. 4) are displaced far to the right. These results would correspond to ice almost 30°C colder than the average temperature of the ice shelf and are clearly not realistic.

The solid line of slope $n = 3$ (Fig. 3) is in reasonable agreement with all the data presented in Figure 3. Increased scatter in the data limited us from using all the points to estimate A and n. The points of which we are less certain tend to fall to the right of the regression line drawn through the best data, indicating that we have underestimated the magnitude of σ_b for many of these less certain points. This is not surprising; bottom crevasses tend to form downstream of pinning points where the magnitude of σ_b is reduced so that stations far-removed from crevasse fields might be expected to exhibit larger magnitudes of σ_b than we estimated.

In summary, our analysis of data from the Ross Ice Shelf is in good agreement with a constitutive relation between the power law and creep for glacier ice with exponent equal to 3. The constant in the constitutive relation, A, averaged over depth for central regions of the Ross Ice Shelf, is 2.3×10^{-25} sec^{-1} (N m^{-2})$^{-3}$. Back stresses ranging up to 0.3 MN m^{-2} or higher, caused by the interaction of the ice shelf with pinning points and with its sides, are an important factor in ice-shelf dynamics (*13*).

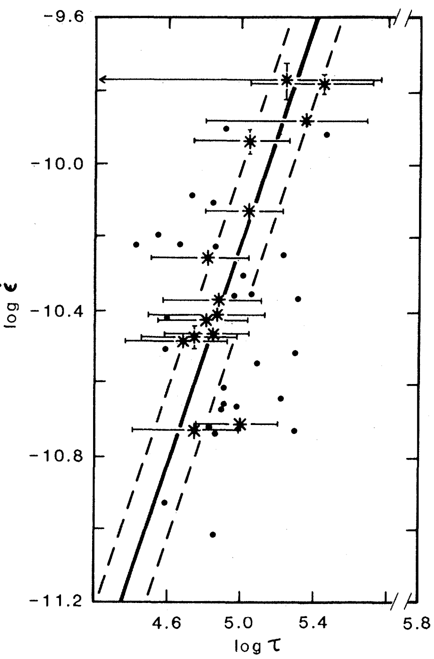

Fig. 3. Log $\dot{\epsilon}$ from surface strain-rate measurements plotted as a function of log τ from bottom crevasse data. The stars correspond to our best estimates of back stress. The circles represent points in which we are less confident. The three lines each have slope $n = 3$. The intercept of the solid line with the vertical axis corresponds to our best estimate of A. The dashed lines show the variations in intercept corresponding to 1 standard deviation in A.

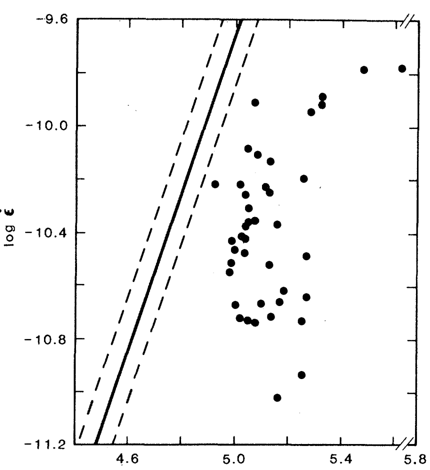

Fig. 4. Log $\dot{\epsilon}$ plotted as a function of values of log τ. A line with slope $n = 3$ fit to these data would result in an intercept corresponding to a temperature 30°C colder than the average ice-shelf temperature.

KENNETH C. JEZEK
U.S. Army Cold Regions Research and Engineering Laboratory, Hanover, New Hampshire 03755
RICHARD B. ALLEY
Geophysical and Polar Research Center, University of Wisconsin, Madison 53706
ROBERT H. THOMAS
Oceanic Processes Branch, National Aeronautics and Space Administration, Washington, D.C. 20546

References and Notes

1. R. LeB. Hooke, *Rev. Geophys. Space Phys.* **19**, 664 (1981).
2. J. Weertman, *Annu. Rev. Earth Planet. Sci.* **11**, 215 (1983).
3. W. S. B. Paterson, *The Physics of Glaciers* (Pergamon, Oxford, ed. 2, 1981).
4. P. J. Martin and T. J. O. Sanderson, *J. Glaciol.* **25**, 33 (1980).
5. J. Weertman, *ibid.* **3**, 38 (1957).
6. R. H. Thomas, *ibid.* **12**, 55 (1973).
7. ______, *ibid.* **24**, 273 (1979).
8. ______ and D. R. MacAyeal, *ibid.* **28**, 397 (1982).
9. K. C. Jezek, *J. Geophys. Res.* **89**, 1925 (1984).
10. J. Weertman, *J. Glaciol.* **25**, 185 (1980).
11. K. C. Jezek and C. R. Bentley, *ibid.* **29**, 118 (1983).
12. R. H. Thomas, D. R. MacAyeal, D. H. Eilers, D. R. Gaylord, in *The Ross Ice Shelf: Glaciology and Geophysics, Antarctic Research Series* (American Geophysical Union, Washington, D.C., in press).
13. T. J. Hughes, *Ann. Glaciol.* **3**, 146 (1982).

14. We thank C. R. Bentley for many helpful suggestions. K.C.J. particularly acknowledges the support of CRREL. Supported by NSF grant DPP-8306689.

23 July 1984; accepted 3 December 198'